Meteorol Atmos Phys 93, 255–273 (2006)
DOI 10.1007/s00703-005-0164-5

Meteorology and Atmospheric Physics
Printed in Austria

[1] Department of Atmospheric Sciences, Yonsei University, Seoul, Korea
[2] School of Earth and Environmental Sciences, Seoul National University, Seoul, Korea

Seasonal variations of gravity waves revealed in rawinsonde data at Pohang, Korea

H.-Y. Chun[1], **I.-S. Song**[1], and **J.-J. Baik**[2]

With 12 Figures

Received March 11, 2004; revised February 2, 2005; accepted April 25, 2005
Published online: May 2, 2006

Summary

Seasonal variations of gravity wave characteristics are investigated using rawinsonde data observed at Pohang observatory, Korea (36°2′N, 129°23′E) during the one-year period of 1998. Analysis is carried out for two atmospheric layers representing the troposphere (2–9 km) and stratosphere (17–30 km). There exist clear seasonal variations in amplitudes of temperature and wind perturbations and wave energy in the stratosphere, with their maxima in wintertime and minima in summertime. A strong correlation is found between the wave activity and the strength of the jet stream, but there is no clear correlation between the wave activity and the vertical gradient of static stability. The intrinsic frequency and vertical and horizontal wavelengths of gravity waves in the stratosphere are $2f$–$3f$, where f is the Coriolis parameter, and 2–3 km and 300–500 km, respectively. The intrinsic phase velocity directs westward in January and northeastward in July. The vertical flux of the stratospheric zonal momentum is mostly negative except in summertime with a maximum magnitude in January. Topography seems to be a major source of stratospheric gravity waves in wintertime. Convection can be a source of gravity waves in summertime, but it is required to know convective sources at nearby stations, due to their intermittency and locations relative to floating balloons.

1. Introduction

Since Leovy (1964) showed that the inconsistency between observed and model-predicted temperature and wind fields near the mesopause can be effectively alleviated by incorporating Rayleigh friction in the zonal momentum equation, many following studies (Holton and Wehrbein, 1980; Lindzen, 1981; Matsuno, 1982) have pointed out that the deposition of gravity wave momentum into the zonal mean flow is a major physical process, which was crudely represented by Rayleigh friction. These studies also pointed out that parameterization of gravity wave drag is required in large-scale numerical models for realistic simulations of the middle atmosphere circulation. Parameterizations of gravity wave drag have been developed actively during the last two decades (e.g., Holton, 1983; Hines, 1991; Fritts and Lu, 1993; Medvedev and Klaassen, 1995; Warner and McIntyre, 1996; Norton and Thuburn, 1999), and most of them require parameters related to wave characteristics, which should be determined from observations.

Rawinsonde data are a valuable resource for gravity wave research due to their extensive geographical and temporal coverage. Kitamura and Hirota (1989) characterized inertia-gravity waves using operational rawinsonde data with a vertical resolution of about 1 km over Japan. Their results show that the wave activity is maximum near the sub-tropical and extra-tropical tropopauses in wintertime due to its connection with the

strength of the subtropical jet and that the waves propagate mainly northwestward with dominant vertical wavelengths of 2–5 km. Recently, gravity waves in the lower stratosphere were studied using high vertical resolution (∼50 m) radiosonde or rawinsonde data collected not only during a few months of intense observational campaigns (e.g., Tsuda et al, 1991; Karoly et al, 1996) but also during several years of routine operation (e.g., Allen and Vincent, 1995; Ogino et al, 1999; Vincent and Alexander, 2000; Wang and Geller, 2003). Long-term, high vertical resolution data are an invaluable resource for investigating seasonal and interannual variations of gravity waves in the lower stratosphere. Allen and Vincent (1995) examined seasonal and latitudinal variations of gravity wave activity using radiosonde data at 18 stations in Australia. The maximum wave activity in the stratosphere was observed in association with convection during the wet season at low latitudes and fronts during the wintertime in midlatitude. Using operational rawinsonde data for 7 years in Japan, Ogino et al (1999) showed interannual and daily variations of gravity wave activity in the lower stratosphere. They showed that the large amplitude of temperature perturbation in wintertime near 20 km altitude at 40° N is strongly correlated with zonal wind near the surface and that this is mainly due to mountain waves induced by strong surface wind in wintertime. Vincent and Alexander (2000) investigated seasonal and interannual variations of gravity wave activity and wave parameters using 5-year rawinsonde data at Cocos Island. They showed that the wave activity is maximum in wet seasons and that the wave energy propagates upward and eastward against prevailing easterlies. Dominant vertical and horizontal wavelengths were about 2 km and 1000 km, respectively, with intrinsic periods of 20–25 hours. Wang and Geller (2003) examined spatial and temporal (seasonal and interannual) variations of gravity wave energy derived using 4-year (1998–2001) U.S. high vertical resolution rawinsonde data. They found that strong troposphere (stratosphere) wave activities exist over the Rocky Mountains (the southern United States) and that the wave energies exhibit interannual variability, which seems to be caused by Quasi-Biennial Oscillation and El Niño-Southern Oscillation. Recently, an attempt to document the climatology of gravity wave parameters in the lower stratosphere was made through the SPARC (Stratospheric Processes and Their Role in Climate) gravity wave initiative using high vertical resolution rawinsonde data in the globe (Vincent, 2003).

This study aims at investigating gravity wave characteristics and their seasonal variations using rawinsonde data observed at Pohang observatory in Korea. In Sect. 2, the rawinsonde data and analysis method are described. In Sect. 3, analysis results including gravity wave energy, wave phase velocity, and momentum flux are presented. Possible mechanisms that cause seasonal variations of wave activity and wave characteristics are also discussed, based on wave sources and background wind and stability conditions. Summary and conclusions are given in the last section.

2. Data and analysis method

There are four meteorological stations in Korea where rawinsondes are launched twice a day (00 UTC and 12 UTC). Data measured by the Vaisala Digicora2 MW15 rawinsonde at Pohang observatory (36°2′N, 129°23′E) are used for this study. The geographical location of Pohang observatory is shown in Fig. 1. Raw data over one year

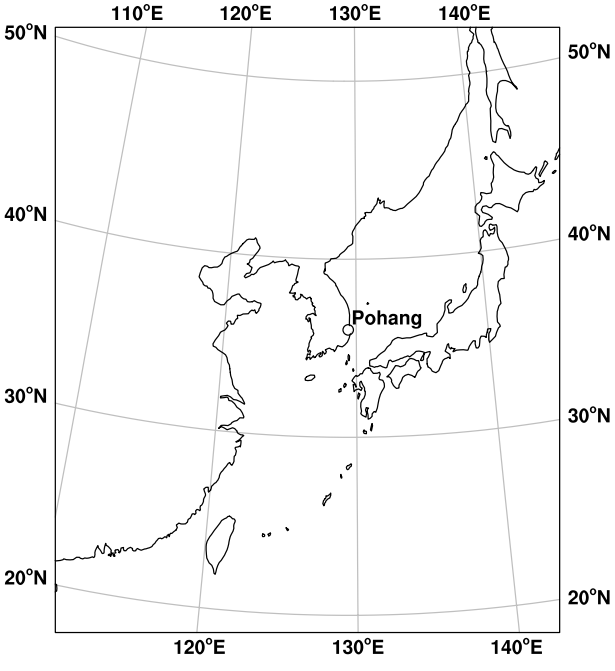

Fig. 1. Geographical location of Pohang rawinsonde observatory (36°2′ N, 129°23′ E)

Table 1. Numbers of available and analyzed rawinsonde profiles in each month. Numbers in parentheses denote numbers of additional soundings obtained during the intense observational campaign KOMEX

Month	Number of available profiles	Number of profiles used for analysis	
		Stratosphere	Troposphere
January	62	24	60
February	56	29	53
March	62	41	60
April	59	40	57
May	60	42	59
June	22(36)	15	21
July	7(38)	31	42
August	32	24	29
September	42	33	41
October	62	46	60
November	60	50	58
December	50	27	49
Total	**574(619)**	**402**	**589**

period (1998) were available only at Pohang observatory. Temperature, wind speed and direction, and dew point temperature were recorded in 10-second intervals and corresponding vertical resolution is approximately 50–60 m considering an ascent rate of 5–6 m s^{-1}. Even though the wind speed and direction were recorded in 10-second intervals, those were interpolated using 100-second smoothed values to reduce observational errors. Consequently, the actual vertical resolution of wind data is about 500–600 m. The number of available soundings in each month is listed in Table 1. Missing data are relatively large in summertime (June to August) and in September. In July, only 7 soundings were available at Pohang. This situation was overcome by including 38 soundings launched at Pohang observatory during the intense observational campaign KOMEX (Korea Monsoon Experiment) (Korea Meteorological Administration, 2000). All sounding data were interpolated in 50-m evenly-spaced vertical intervals up to the height reached by rawinsondes.

In this study, the analysis of wave perturbations is carried out for two atmospheric layers representing the troposphere and stratosphere. The upper limit of the troposphere is chosen based on the tropopause height at Pohang observatory (Chun and Song, 2001), which revealed mean tropopause heights of 10–11 km in wintertime and 14–16 km in summertime. The strong seasonal variation of midlatitude tropopause height contrasts with nearly constant tropopause heights found in low-latitude regions as reported in Allen and Vincent (1995) and Vincent and Alexander (2000). In order to avoid erroneous effects on power spectrum due to the presence of an inversion layer near the top of the planetary boundary layer and a sudden increase of static stability near the tropopause, two fixed layers of $z = 2$–9 km and 17–30 km are chosen to represent the troposphere and stratosphere, respectively. Temperature or wind perturbation is defined by subtracting a basic-state profile in each layer from each sounding. The basic-state profile in each layer is obtained by fitting a second-order polynomial using the least-square method. A higher-order polynomial fitting (third- or fourth-order) did not make any significant difference in the calculated perturbations.

3. Results and discussion

Figure 2 shows the vertical profiles of temperature, zonal wind, and meridional wind perturbations and the hodograph of wind perturbations in the stratosphere and troposphere at 00 UTC 8 May 1998. In the stratosphere, dominant vertical wavelength is about 1.5 km in the region of $z = 20$–25 km and about 3 km elsewhere. The maximum perturbations of temperature, zonal wind, and meridional wind are about 4 K, 4 m s^{-1}, and 7 m s^{-1}, respectively. The elliptical shape of the hodograph and the anticyclonic rotation of horizontal wind with height indicate that the observed wind perturbations can be regarded as upward-propagating inertia-gravity waves. There are approximately six wave cycles in the elliptical hodograph in the stratospheric layer. All six cycles rotate anticyclonically with height, implying that gravity waves are generated by wave sources below $z = 17$ km and transport their energy upward. The major axis of the ellipse, indicative of the horizontal propagation direction of gravity waves, is approximately in the south-southeast to north-northwest direction in the stratosphere. The exact direction of wave propagation will be determined later with a polarization relationship between wind and temperature perturbations. The magnitudes of wind

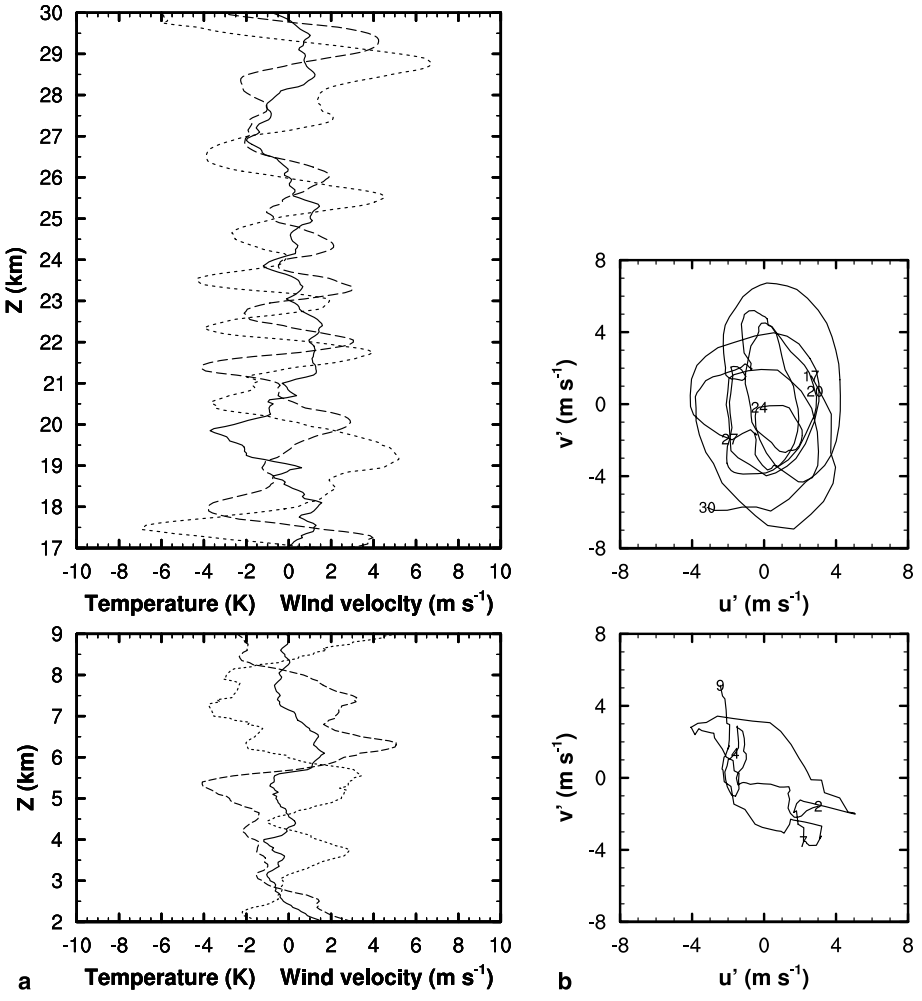

Fig. 2a. Vertical profiles of temperature (solid line), zonal wind (dashed line), and meridional wind (dotted line) perturbations, and (**b**) hodograph of wind perturbations at 00 UTC 8 May 1998. The upper figures are for the stratosphere (17–30 km) and the lower figures are for the troposphere (2–9 km). The numbers in the hodograph indicate heights in km

and temperature perturbations are smaller in the troposphere than in the stratosphere. Downward energy propagation is evidenced by the cyclonic rotation of the hodograph in the regions of $z = 4$–5 km and $z = 7$–7.5 km.

Figure 3 shows the monthly-averaged root-mean-square amplitudes of temperature, zonal wind, and meridional wind perturbations in the stratosphere and troposphere. In the stratosphere, seasonal variations of wind and temperature perturbations are clearly indicated (maximum values of $3.9\,\mathrm{m\,s^{-1}}$ and $2.0\,\mathrm{K}$ in wintertime and minimum values of $1.6\,\mathrm{m\,s^{-1}}$ and $0.9\,\mathrm{K}$ in summertime). The magnitude of wind perturbation in wintertime is larger than that reported by Kitamura and Hirota (1989) (2–$3\,\mathrm{m\,s^{-1}}$), while the magnitude of temperature perturbation is similar to that in their study. The root-mean-square amplitudes of perturbations are smaller in the troposphere than in the stratosphere. In the troposphere, there are no clear seasonal variations in the amplitudes.

3.1 Wave energy

Wave activity can be estimated by calculating wave energies per unit mass defined by

$$E_T = E_k + E_p = \frac{1}{2}\left[\overline{u'^2} + \overline{v'^2} + \overline{w'^2}\right] + \frac{1}{2}\left[\frac{g^2}{N^2}\overline{\left(\frac{T'}{\overline{T}}\right)^2}\right], \quad (1)$$

where E_T, E_k, and E_p are the total, kinetic, and potential energies per unit mass, respectively, u', v', w', and T' are the zonal wind, meridional wind, vertical wind, and temperature perturbations, respectively, $\overline{T}$ is the basic-state temperature, N is the buoyancy frequency, and g is the gravitational acceleration. In (1), the overbar indicates a vertical average over each layer. Since

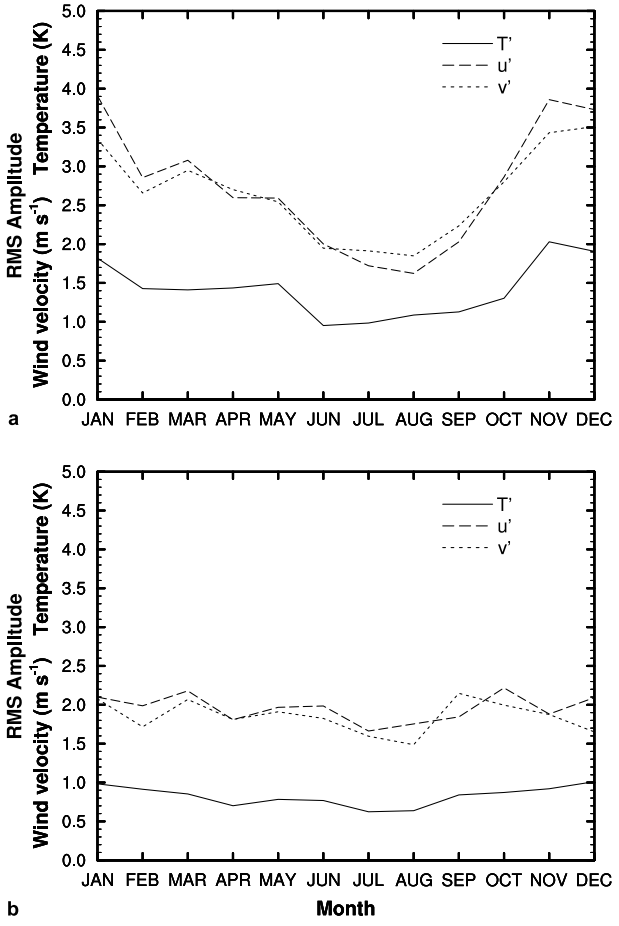

Fig. 3. Time series of monthly-averaged root-mean-square amplitudes of temperature (solid line), zonal wind (dashed line), and meridional wind (dotted line) perturbations in the (**a**) stratosphere, and (**b**) troposphere

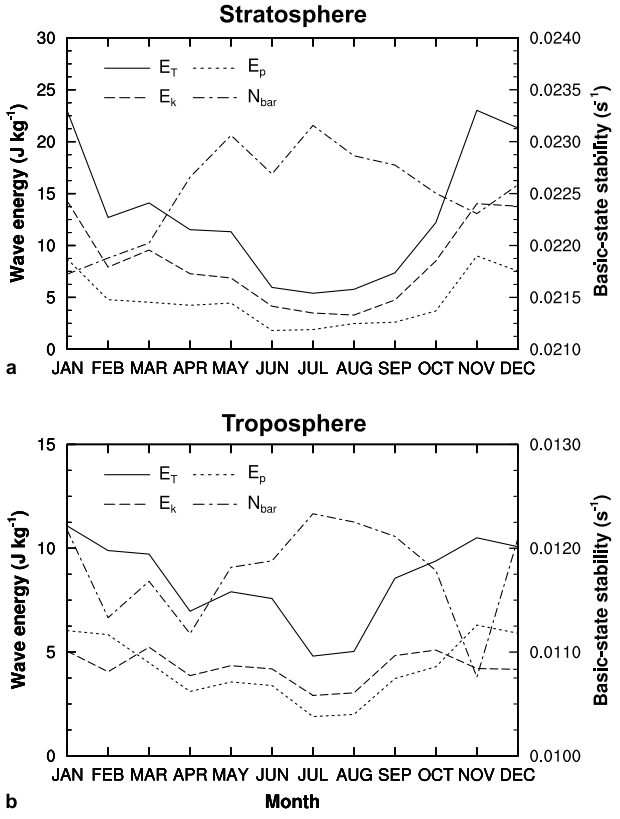

Fig. 4. Time series of monthly-averaged E_T (solid line), E_k (dashed line), E_p (dotted line), and N (dot-dashed line) in the (**a**) stratosphere, and (**b**) troposphere

the vertical wind is not measured by rawinsonde, E_k in (1) is calculated without vertical wind component.

Figure 4 shows monthly-averaged E_T, E_k, E_p, and N. The maximum and minimum E_T are observed in January and July, respectively, in both the stratosphere and troposphere. Seasonal variation of wave energies clearly appears in the stratosphere, while it is relatively less obvious in the troposphere. In the stratosphere, strong seasonal variation of wave energies is due to that of the root-mean-square amplitudes of wind and temperature perturbations as well as Brunt-Vaisala frequency (see Figs. 3a and 4a). In the troposphere, variation of wave energy is mainly due to the root-mean-square amplitudes of the normalized temperature perturbation (not shown) rather than the root-mean-square amplitudes of wind and temperature perturbations (Fig. 3b). This is because the root-mean square of the normalized temperature perturbation has a clear seasonal variation (stronger in January, November, and December and weaker in April, July, and August), which influences seasonal variation of E_p along with seasonal variation of the Brunt-Vaisala frequency.

In previous studies, strong seasonal variations of wave perturbations and wave energy were reported and possible mechanisms for this were proposed. Using rawinsonde data over Japan, Kitamura and Hirota (1989) showed that large perturbations in wintertime are correlated to the strength of the subtropical jet near the tropopause. Eckermann (1995) suggested a simple wave model for estimating wind and temperature variances based on both monochromatic-wave and multi-wave spectral theories under the assumption of constant basic-state wind and source strength. He showed that seasonal variations of wind and temperature perturbations below 60 km height are mainly due to the seasonal variations of density stratification and Brunt-Vaisala

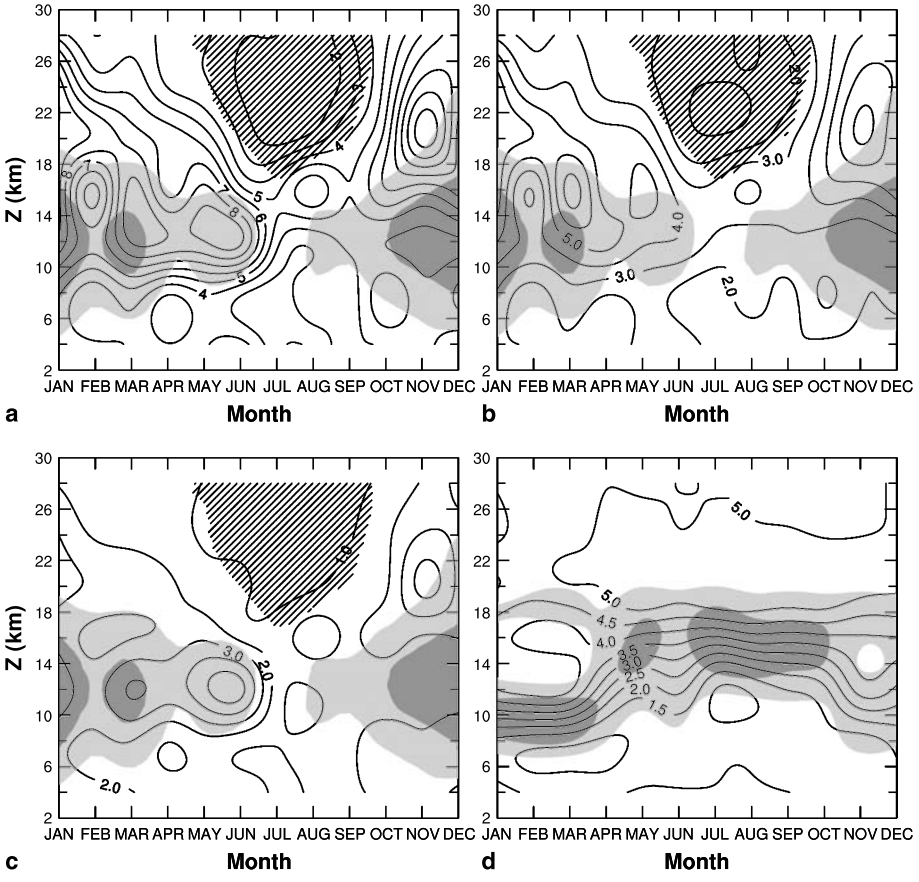

Fig. 5. Time-height cross-section of monthly-averaged (**a**) E_T, (**b**) E_k, (**c**) E_p, and (**d**) N^2. The contour interval is $1\,\mathrm{J\,kg^{-1}}$ in (**a**)–(**c**) and $0.5\times10^{-4}\,\mathrm{s^{-2}}$ in (**d**). In (**a**)–(**c**), regions of monthly-mean westerly flow larger than $25\,\mathrm{m\,s^{-1}}$ ($45\,\mathrm{m\,s^{-1}}$) are lightly (darkly) shaded, and easterly regions are hatched. In (**d**), regions of $\mathrm{d}N^2/\mathrm{d}z > 2\times10^{-8}\,\mathrm{s^{-2}\,m^{-1}}$ ($5\times10^{-8}\,\mathrm{s^{-2}\,m^{-1}}$) are lightly (darkly) shaded. The raw data are smoothed by contour plotting program

frequency, respectively. Allen and Vincent (1995), using radiosonde data in Australia, suggested that the maximum wave energy near the tropopause is related to the strong vertical gradient of N^2 there. Ogino et al (1999) suggested that the large amplitude of temperature perturbation in wintertime near 20 km height at 40° N is mainly due to the enhanced mountain waves induced by strong surface wind.

To examine possible mechanisms for causing seasonal variation of wave energy in this study, the time-height cross-section of monthly-averaged E_T, E_k, E_p, and N^2 is shown in Fig. 5. Here, contours of wave energies and N^2 are overlaid on shaded and hatched plots of monthly-averaged zonal wind and the vertical gradient of N^2, respectively. The wave energies are calculated in each 4-km bin (2–6, 6–10, ..., 26–30 km) using perturbations that are obtained by subtracting a basic-state (second-order polynomial form) of each 4-km bin. Then, monthly and vertically averaged energy over each 4-km bin is assigned at the middle level of 4 km bin. A region of maximum E_T, E_k, and E_p is located at $z = 10$–18 km in March–June. This region roughly corresponds to the jet stream region (shaded regions in Fig. 5a–c). However, in January, November, and December, a region of maximum E_T, E_k, and E_p is centered near $z = 21$ km, which is far above the major jet stream region ($z \sim 12$ km). The wave energy is minimum above $z = 18$ km during June–October in the easterly zonal wind region (hatched regions in Fig. 5a–c). This indicates that gravity waves generated in the troposphere cannot propagate into the summer stratospheric region with easterly zonal wind. That is, stationary waves induced by mountains might be absorbed near a critical level, where the zonal wind becomes zero, and hence only a small portion of wave energy is observed in the stratosphere.

There is no clear positive or negative correlation between the wave energies and the strength of the vertical gradient of N^2. This result is in contrast to that of Allen and Vincent (1995). In particular, the vertical gradient of N^2 is very small above $z = 20$ km where the wave energy is large in wintertime. In order to check whether

the large amplitude of wave energy in wintertime above $z = 20$ km shown in Fig. 5 is related to mountain waves as suggested by Ogino et al (1999), the time series of total wave energy averaged in 18–22 km height range in December and zonal wind averaged in every 3 km altitude range from 0 to 30 km were plotted (not shown). The strong positive correlation between the wave energy averaged in 18–22 km height range and the zonal wind near the surface as shown in Ogino et al is not clearly seen in the present case. This may not imply that the mountain is not a main source of gravity waves observed at Pohang observatory that is located in the eastern coast of Korea. There are several mountains on the west and northwest of Pohang observatory. The prevailing low-level wind on the upstream of Pohang observatory in wintertime can vary depending on synoptic situations. When a high-pressure system centered in continent of China extends to the east coast of Korea, northerly or northeasterly flow is dominant below about 850 hPa and reverses its direction above that. In this case, there is no chance to detect mountain waves at Pohang observatory in the stratosphere due to critical-level filtering. When a low-pressure system occupies Korea, northwesterly or southwesterly is dominant on the upstream of Pohang observatory at low level, and westerly above. In this case, vertically propagating mountain waves with horizontal wavelengths less than $2\pi|U|/f$ (in the case of hydrostatic waves), where $|U|$ is the magnitude of westerly jet, can go through westerly jet, and they may be detected at Pohang observatory above $z = 17$ km. This is possible only when the background wind is not so strong to drift balloons far from regions of mountain wave activity. As will be shown in Figs. 8 and 9, soundings having northwesterly low-level wind show near-zero ground-based phase velocity, while those having northeasterly flow show large magnitude of ground-based phase velocity.

There might be other possibilities for the large amplitude of gravity wave energy above $z = 20$ km in wintertime at Pohang observatory. One possibility is the transport of gravity wave energy from the equatorial tropopause as shown by Sato et al (1999) using high-resolution GCM results. They showed that there is poleward and upward energy transport from the tropical tropopause by short-period (less than 24 hr) gravity waves and small vertical-scale (less than 5 km) gravity waves, even though the latter is less clear with equatorward energy transport just above the subtropical jet. Considering that the dominant vertical wavelength of waves analyzed in the present study is less than 5 km (Figs. 7a, b), the present results are more applicable to the small-vertical scale disturbance by Sato et al (1999). Based on the calculation of $\overline{v'w'}$ for individual soundings in the present study, which will be presented in Subsect. 3.4, there is, however, no clear signal of anisotropy of wave propagation in meridional direction, especially in wintertime. 13 (17) among 24 (29) soundings in January (July) have positive sign of $\overline{v'w'}$, indicating northward and upward wave propagation. Thus, it is hard to speculate that the large amplitude of gravity wave energy above $z = 20$ km in wintertime may be transported from the equatorial tropopause.

Cumulus convection can be another source of gravity waves that have wide phase speed spectrum, and thus convectively forced gravity waves can propagate to the stratosphere more easily, compared with mountain waves, under various basic-state wind conditions. In summertime, there exists strong convective activity in Korean peninsula associated with Asian monsoon circulation and typhoons passing through or near this area. Thus, one can expect a large value of wave energy due to convectively forced gravity waves in the summer stratosphere. However, the observed wave energy is minimum in summertime not only by the monthly mean value (Fig. 5) but also by individual sounding (not shown). This result is somewhat unexpected, even considering relatively large missing data in summertime. One possible reason for this is the limitation of observing frequency (twice daily) and analysis depth in rawinsonde data, which can be especially pronounced for waves generated by intermittent sources such as convective clouds. Alexander and Holton (2004) nicely showed that the characteristics of observed gravity waves generated by transient convective sources depend strongly on the location and timing of observation from convective sources. Through simple linear numerical modeling, they showed that waves with very large vertical wavelengths and high phase speeds exist only for a short period of time close to convective sources, and accordingly waves observed in operational radiosondes or

rawinsondes are likely to have low frequencies and short vertical wavelengths. This observational selection of convectively forced gravity waves will be discussed in detail in Sect. 3.5.

Even though the above arguments in the time-height distribution of gravity wave energy are based on wave sources and dissipation mechanisms, it should be noticed that gravity wave energy cannot be conserved during propagation, even without momentum flux dissipation. The total gravity wave energy can be changed with time in the presence of a basic-state wind shear by the exchange of energy between the wave and the mean flow, even with constant momentum flux (Andrews et al, 1987). In general, it seems to be, however, very difficult to quantify this conservative shear change in wave energy density with observational data since this depends on parameters like phase speed and momentum flux, which are hard to be estimated from data. Furthermore, the wave energy calculated over 4 km-height bin is highly affected by observational selection of waves. In the presence of strong wind shear, waves will be Doppler-shifted in and out of the window and seasonal variations of wave energy observed by rawinsonde are not necessarily related to those of wave sources.

3.2 Characteristic vertical wavenumber

The vertical wavenumber for the largest contribution to the total wave energy is a characteristic wavenumber (m_*), which is one of the important parameters in the gravity wave drag parameterization based on Fritts and VanZandt (1993). Following Allen and Vincent (1995), the monthly-averaged m_* and spectral slope (t) from the monthly-averaged power spectrum are calculated using the Levenberg-Marquardt nonlinear regression method (Press et al, 1992) with a fitting curve of

$$F(m) = F_0 \frac{m/m_*}{1 + (m/m_*)^{t+1}}, \tag{2}$$

where m is the vertical wavenumber resolvable in the monthly-averaged power spectrum and F_0 is a constant. The monthly-averaged power spectral density is calculated for normalized temperature perturbation ($T'/\overline{T}$) in the stratosphere and troposphere (not shown). Since the analysis depth of the stratosphere (troposphere) is 13 km (7 km) and the vertical resolution of data is 50 m, the resolvable vertical wavelength ranges from 100 m to 13 km (from 100 m to 7 km) in the stratosphere (troposphere). In order to reduce the leakage of spectral density to neighboring wavenumbers, a Welch window is applied to the normalized temperature perturbation before taking a Fourier transform. The spectral density at some highest wavenumbers is affected by the window function employed in a spectral analysis. In the stratosphere, a correction of power spectrum by sensor response time is made following Allen and Vincent (1995). This correction generally makes the total var-

Table 2. Monthly-averaged characteristic vertical wavenumber (m_*) (wavelength) and spectral slope (t)

Month	m_* (cycles m^{-1}) (wavelength, km)		t	
	Stratosphere	Troposphere	Stratosphere	Troposphere
January	2.18×10^{-4} (4.59)	2.50×10^{-4} (4.00)	2.84	2.96
February	2.81×10^{-4} (3.56)	2.08×10^{-4} (4.81)	2.76	2.84
March	2.37×10^{-4} (4.22)	2.77×10^{-4} (3.61)	2.60	2.91
April	2.46×10^{-4} (4.07)	2.70×10^{-4} (3.70)	2.74	2.88
May	1.65×10^{-4} (6.06)	2.58×10^{-4} (3.88)	2.39	2.72
June	2.74×10^{-4} (3.65)	2.38×10^{-4} (4.20)	2.81	2.87
July	1.78×10^{-4} (5.62)	2.82×10^{-4} (3.55)	2.48	2.74
August	1.73×10^{-4} (5.78)	3.21×10^{-4} (3.12)	2.49	2.85
September	2.31×10^{-4} (4.33)	2.49×10^{-4} (4.02)	2.61	2.80
October	2.44×10^{-4} (4.10)	2.72×10^{-4} (3.68)	2.68	2.89
November	2.47×10^{-4} (4.05)	1.91×10^{-4} (5.24)	2.81	2.78
December	2.24×10^{-4} (4.46)	2.47×10^{-4} (4.05)	2.69	3.06
Mean	**2.27×10^{-4} (4.54)**	**2.55×10^{-4} (3.99)**	**2.66**	**2.86**

iance of the power spectrum increase slightly and the spectral slope on the short-wavelength tails decrease.

The monthly-averaged characteristic vertical wavelength ($\lambda_* = 2\pi/m_*$) and spectral slope in the stratosphere and troposphere are listed in Table 2. The annual mean of λ_* is 4.54 km in the stratosphere and 3.99 km in the troposphere. Even though seasonal variation of characteristic wavelength is not so obvious in both the stratosphere and troposphere, the characteristic wavelength tends to be larger (smaller) in summertime than in wintertime in the stratosphere (troposphere). The spectral slope in the stratosphere is consistently smaller than 3 with an annual mean of 2.66, while it is close to 3 (an annual mean of 2.86) in the troposphere. The spectral slopes close to 3 are consistent with results in previous observational studies (e.g., VanZandt, 1982; Dewan et al, 1984; Tsuda et al, 1991; Allen and Vincent, 1995). This result has also been evidenced by linear and nonlinear wave saturation theories (e.g., Dewan and Good, 1986; Weinstock, 1990; Hines, 1991). However, the spectral slope of 3 is not always expected. In fact, several exceptional cases have been reported, especially when specific wave sources or unsaturated waves in a strong shear flow are considered (Fritts and Alexander, 2003).

3.3 Wave propagation

The mean horizontal propagation direction of gravity waves is calculated using

$$\phi = \tan^{-1}(y/x),$$
$$x = \overline{u'T'_{+90}}, \qquad y = \overline{v'T'_{+90}}, \tag{3}$$

where ϕ is the azimuth of propagation measured counterclockwise from the east. In (3), T'_{+90} denotes the temperature perturbation whose all spectral components are shifted by $+90°$. This can be achieved by the Hilbert transform of temperature perturbation (Vincent et al, 1997). The computed propagation directions are grouped into 30° angular segments. The contribution of soundings included in each 30° angular segment to the total wave energy is calculated by

$$\Phi_i = \frac{\sum_j E_j(i)}{E_{\text{total}}}, \tag{4}$$

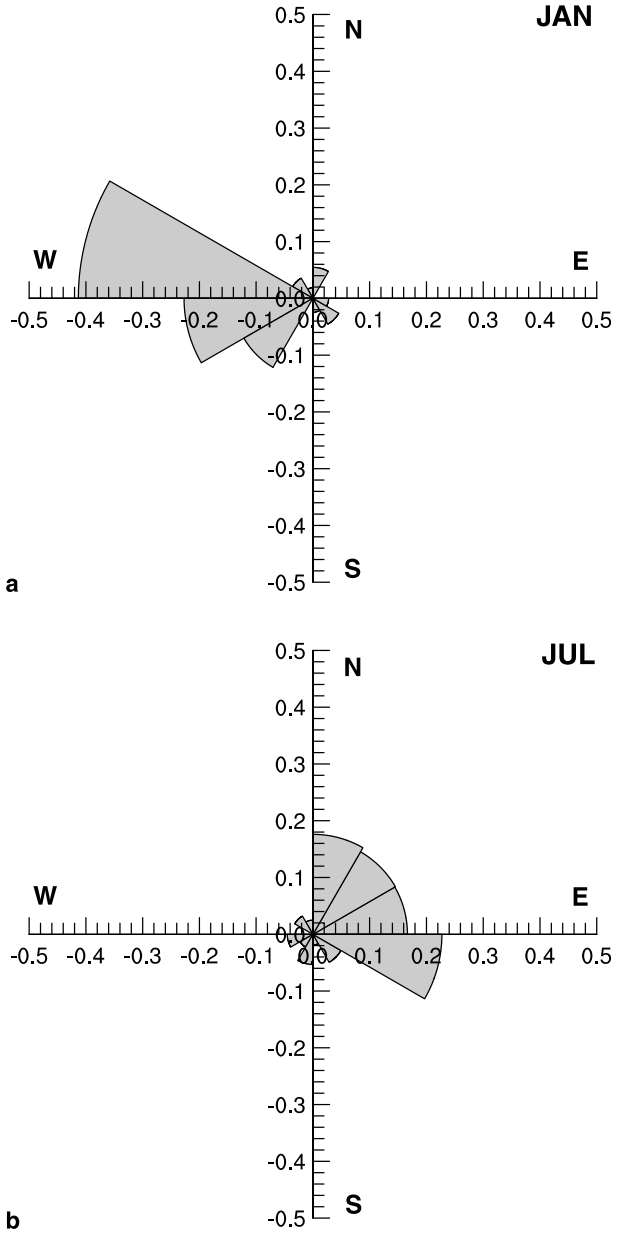

Fig. 6. Histogram of mean direction of horizontal wave propagation in the stratosphere in (**a**) January, and (**b**) July

where $E_j(i)$ is the total wave energy defined in (1) by the j-th sounding in the i-th segment and E_{total} is the total wave energy calculated using all soundings. Figure 6 shows the histogram of mean propagation direction in the stratosphere in January and July. Gravity waves propagate mainly westward in wintertime and east-northeastward in summertime. This figure indicates that there exists a strong anisotropy of wave propagation direction in the midlatitude stratosphere. This anisotropy was also found in the tropical case by Vincent et al (1997). In the tro-

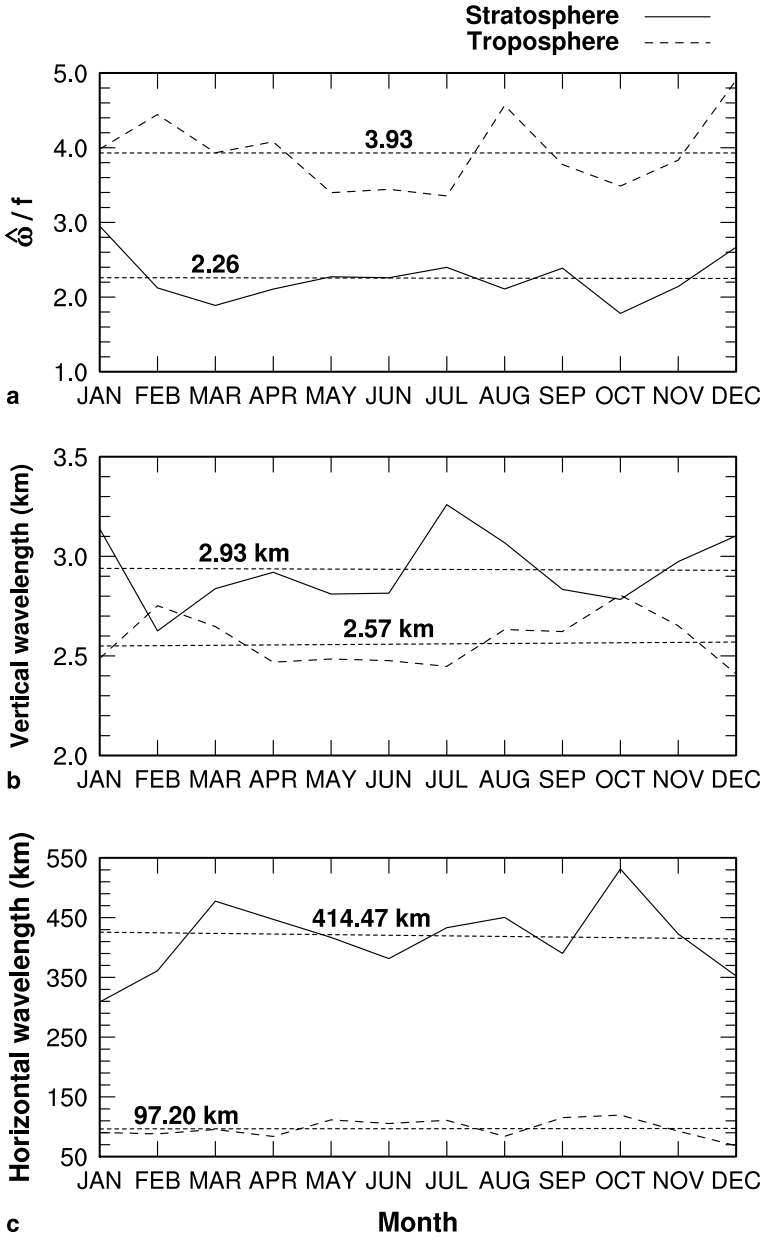

Fig. 7. Time-series of monthly-averaged (**a**) $\hat{\omega}/f$, (**b**) vertical wavelength by (6), and (**c**) horizontal wavelength by (5) in the stratosphere. The dotted lines are annual means

posphere (not shown), the directional anisotropy was not evident.

The horizontal wavenumber k_h is obtained using the dispersion relationship of a monochromatic inertia-gravity wave given by

$$k_h{}^2 = \frac{m^2 f^2 \left[(\hat{\omega}/f)^2 - 1\right]}{N^2}. \tag{5}$$

Here, the vertical wavenumber m is calculated by

$$m = \frac{\sum_i (|\hat{u}_i|^2 + |\hat{v}_i|^2) m_i}{\sum_i (|\hat{u}_i|^2 + |\hat{v}_i|^2)}, \tag{6}$$

where $\hat{u}_i$ and $\hat{v}_i$ are the coefficients of the i-th Fourier component of u' and v', respectively, corresponding to the i-th vertical wavenumber (m_i). The intrinsic horizontal phase velocity[1] ($\hat{c}$), ground-based phase velocity ($\underline{c}$),

[1] Note that "phase velocity" in this paper is the speed at which a point of constant phase moves in the direction of wave propagation, which should be distinguished from "phase speed" that is the speed of lines of constant phase. In textbooks and scientific literature, however, we see either phase speed or phase velocity. This terminology problem is discussed by Nappo (2002).

and ground-based group velocity ($\underline{c}_g$) can be obtained by

$$\hat{\underline{c}} = \frac{\hat{\omega}}{k_h}\frac{\underline{k}_h}{k_h}, \tag{7}$$

$$\underline{c} = (\hat{\omega} + \underline{k}_h \cdot \underline{V})\frac{\underline{k}_h}{|\underline{k}_h|^2}, \tag{8}$$

$$\underline{c}_g = \underline{V} + \hat{\underline{c}}_g = \underline{V} + \left(1 - \frac{f^2}{\hat{\omega}^2}\right)\hat{\underline{c}}. \tag{9}$$

Here, $\hat{\omega}$ is the intrinsic frequency, k_h is the horizontal wavenumber, f is the Coriolis parameter, and $\underline{V}$ is the mean horizontal basic-state wind. The intrinsic frequency can be determined from horizontal wind perturbations under the inertia-gravity wave polarization relationship. The ratio of major to minor axis in an ellipse of horizontal wind perturbations is calculated using the Stokes parameter method (Eckermann and Vincent, 1989; Eckermann, 1996). Then, $\hat{\omega}/f$ is obtained from the axial ratio by including the effects of vertical shear of horizontal wind components following Hines (1989).

The time series of monthly-averaged $\hat{\omega}/f$ and horizontal and vertical wavelengths ($2\pi/k_h$ and $2\pi/m$, respectively) in the stratosphere and troposphere are shown in Fig. 7. The annual mean values of $\hat{\omega}/f$ in the stratosphere and troposphere are 2.26 and 3.93, respectively, and corresponding intrinsic periods of dominant waves are 9 and 5.2 hrs, respectively. There is no clear seasonal variation of $\hat{\omega}/f$. The vertical wavelength, obtained from (6), ranges from 2.63 to 3.26 km in the stratosphere with an annual mean of 2.93 km and from 2.41 to 2.81 km with an annual mean of 2.57 km in the troposphere. The monthly-averaged horizontal wavelength in the stratosphere ranges from 309 to 531 km with an annual mean of 414 km. There is no clear signal of seasonal variation of horizontal and vertical wavelengths. In the troposphere, the annual mean of horizontal wavelength is 97 km, which is less than $1/4$ of that in the stratosphere. This is because the buoyancy frequency in the troposphere is about the half of that in the stratosphere and $\hat{\omega}$ in the troposphere is roughly 2 times larger than that in the stratosphere.

Balloon sounding gives an effective vertical profile for waves only when horizontal wavelengths of the waves are larger than the horizontal travel distance of balloon. Therefore, it should be checked whether an estimated horizontal wavelength is valid for the assumption behind the analysis method used in this study. For this, the maximum horizontal displacements of balloons are calculated for the troposphere and stratosphere. The maximum displacement is defined as a maximum value of horizontal distance between two different positions in a horizontal trajectory of balloon. In the troposphere (2–9 km), maximum displacements are mostly smaller than horizontal wavelengths except for 13 cases (among 589 soundings), which occur exclusively in January–March and December when the jet stream is strong. In those 13 cases, maximum displacements are slightly larger than or comparable to horizontal wavelengths. In the stratosphere (17–30 km), such invalid cases do not occur at all.

Figure 8 shows the intrinsic horizontal phase velocity, ground-based phase velocity, and ground-based group velocity in the stratosphere in January and July. Waves mainly propagate westward relative to the basic-state wind in January and northeastward in July. The mean of intrinsic phase velocity is 8.43 m s^{-1} toward the west in January and 7.42 m s^{-1} toward the northeast in July. This seasonal preference of propagation direction is consistent with that of Sato (1994) who showed statistical characteristics of inertia-gravity waves and their sources in the lower stratosphere using three-year MU radar data observed in Japan. In the height range of 18–22 km, she showed that observed gravity waves in wintertime propagate westward relative to the background wind, implying that the mountain is a major source of observed waves that are excited by strong westerly winds near the surface. Based on the meridional propagation direction of wave energy relative to the location of subtropical jet at 200 hPa, she showed that geostrophic adjustment process is unlikely to be a wave source. In the present study, 11 (17) among 24 (29) soundings averaged over the height range of 17–30 km propagate southward (northward) in January (July). This indicates that geostrophic adjustment process at jet axis may not be a wave source in January (July), as consistent with Sato (1994). This is because the jet axis defined by latitude at which the maximum zonal wind exists at 200 hPa, 130° E appeared in 6 hourly National

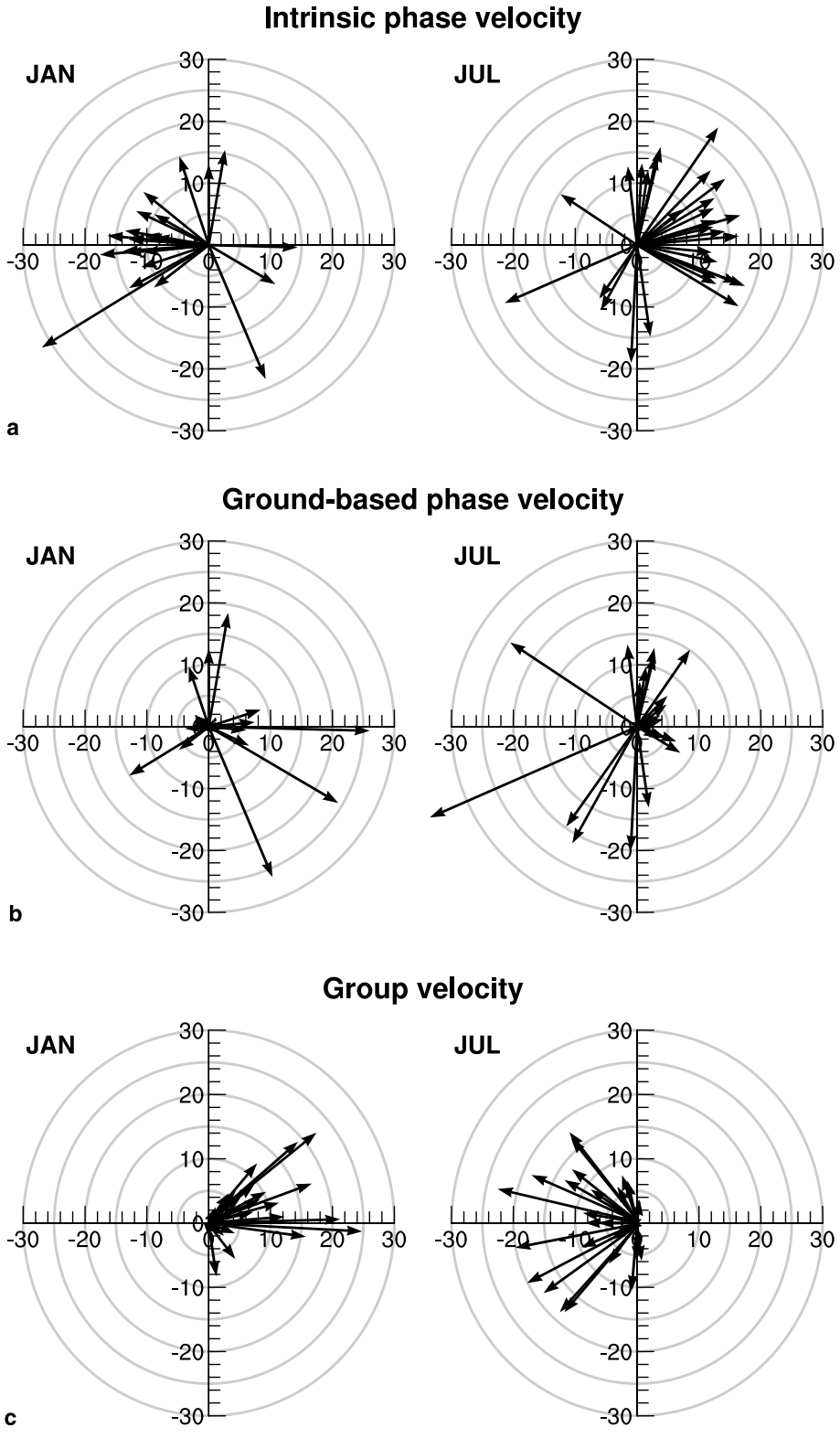

Fig. 8a. Intrinsic phase velocity, (**b**) ground-based phase velocity, and (**c**) ground-based group velocity in January and July. The unit is in m s^{-1}

Centers for Environmental Prediction (NCEP) reanalysis data (not shown) is located mostly at the south (north) of Pohang observatory in January (July) 1998.

The magnitude of ground-based phase velocity is smaller than that of intrinsic phase velocity except for a few soundings. In January, 17 among 24 soundings have very weak phase

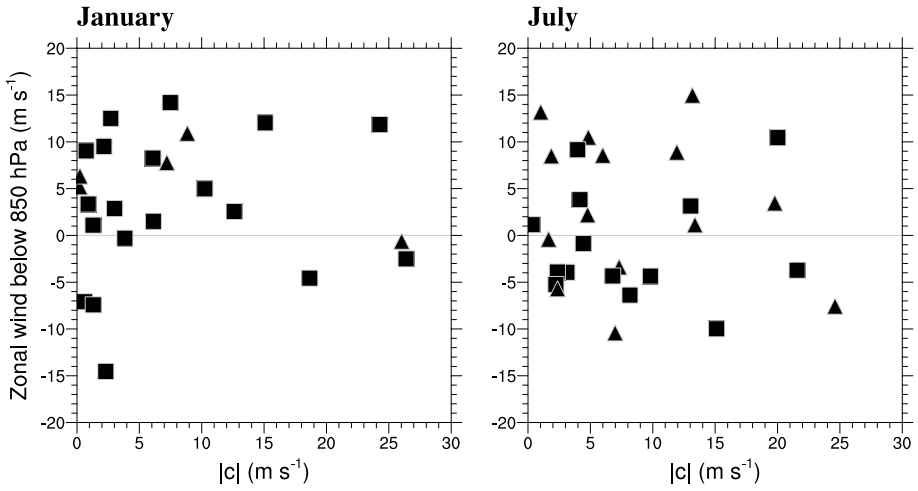

Fig. 9. Scatter diagrams of the observed soundings in January and July projected onto a two-dimensional space of magnitude of ground-based phase velocity and zonal wind in the lower atmosphere (averaged below 850 hPa). The triangle and square symbols denote the positive and negative signs of meridional wind, respectively, so that the squares (triangle) in positive and negative zonal winds indicate northwesterly (southwesterly) and northeasterly (southeasterly), respectively

velocities (less than $10\,\mathrm{m\,s^{-1}}$), implying that topography can be a source of gravity waves in the winter stratosphere. As mentioned earlier, low-level (below about 850 hPa) wind on the upstream of Pohang observatory is either northwesterly or northeasterly in wintertime according to synoptic pressure systems, and mountain waves can be possibly observed above $z = 17$ km when the zonal component of low-level wind is positive. Figure 9 shows scatter diagrams of observed soundings in January and July in a two-dimensional space of the magnitude of ground-based phase velocity and zonal wind in the lower layer (averaged below 850 hPa). The sign of meridional wind is denoted by different symbols, so that wind direction in the lower layer for each sounding can be figured out. In January, 13 among the 17 soundings that have phase velocities of less than $10\,\mathrm{m\,s^{-1}}$ have positive zonal wind, and 10 among those 13 soundings have relatively weak zonal wind speed (less than $10\,\mathrm{m\,s^{-1}}$). The wind with positive zonal wind is mostly (13 among 17 soundings) northwesterly while that with negative zonal wind is mostly (6 among 7 soundings) northeasterly. These results clearly show the possibility that the observed disturbances in the winter stratosphere at Pohang station are mountain-induced gravity waves under favorable synoptic condition of northwesterly with relatively weak low-level wind speed. This is less evident in July. 18 among 28 soundings have phase velocities of less than $10\,\mathrm{m\,s^{-1}}$, but they are rather evenly distributed in the zonal wind space (8 for positive and 10 for negative), unlike in January. The ground-based group velocity is mostly directed northeastward in January and westward in July mainly because the basic-state wind dominates intrinsic group velocity.

Alternatively, any moving or transient sources can possibly induce waves with a zero ground-relative phase speed. However, moving sources such as convective clouds generally generate gravity waves with a broad phase-speed spectrum, and waves observed are a superposition of the spectrum. This raises a question whether it is reliable to infer wave sources based on the calculated value of wave properties in the present study, especially when there are multiple sources and/or there is a spectrum of waves induced by a single source. This is one of the major limitations of the current analysis method that is based on the monochromatic wave assumption.

3.4 Momentum flux

The evidence of the strong anisotropy of wave propagation in Figs. 6 and 8 suggests that there exist a significant amount of momentum flux associated with gravity waves. The magnitude and vertical profile of momentum flux are crucial to the estimation of how much and where gravity waves can influence the large-scale flow. The vertical flux of zonal ($\overline{u'w'}$) and meridional

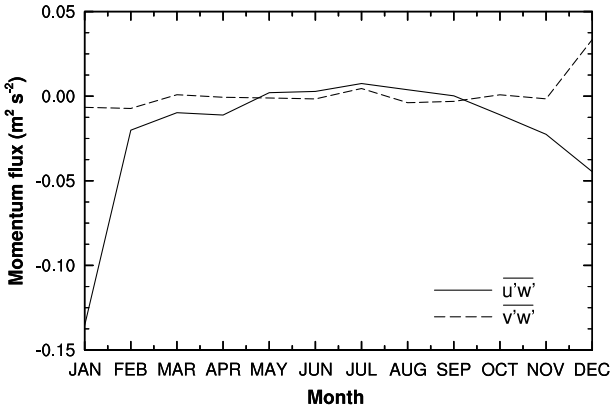

Fig. 10. Time series of monthly-averaged zonal ($\overline{u'w'}$) and meridional ($\overline{v'w'}$) momentum fluxes per unit mass averaged in the stratosphere

($\overline{v'w'}$) momentum per unit mass cannot be calculated directly because w' is not measured by rawinsonde. These quantities, however, can be estimated using the phase relationship between variables through the monochromatic inertia-gravity wave theory. Following Vincent et al (1997), the zonal and meridional momentum fluxes can be expressed by

$$\overline{u'w'} = \frac{g\hat{\omega}}{N^2}\overline{u'\left(\frac{T'}{\bar{T}}\right)_{+90}}\left[1-\left(\frac{f}{\hat{\omega}}\right)^2\right], \tag{10}$$

$$\overline{v'w'} = \frac{g\hat{\omega}}{N^2}\overline{v'\left(\frac{T'}{\bar{T}}\right)_{+90}}\left[1-\left(\frac{f}{\hat{\omega}}\right)^2\right]. \tag{11}$$

Here, $\hat{\omega}$ is given by the intrinsic frequency derived from hodographs of wave perturbations.

Figure 10 shows the time series of monthly-averaged zonal and meridional momentum fluxes per unit mass averaged over $z = 17$–30 km range calculated using $\hat{\omega}$ estimated by the hodograph analysis shown in Fig. 7a. $\overline{u'w'}$ is mostly negative except in summertime. The magnitude of zonal momentum flux in wintertime is much larger ($-0.13\,\mathrm{m^2\,s^{-2}}$ in January, $-0.02\,\mathrm{m^2\,s^{-2}}$ in November, and $-0.04\,\mathrm{m^2\,s^{-2}}$ in December) than that in summertime ($0.002\,\mathrm{m^2\,s^{-2}}$ in May and June, $0.007\,\mathrm{m^2\,s^{-2}}$ in July, $0.003\,\mathrm{m^2\,s^{-2}}$ in August, and $0.0002\,\mathrm{m^2\,s^{-2}}$ in September). In January, magnitude of zonal momentum flux is about 6 times larger than that in November, even though the magnitudes of wave energies (Fig. 4a) in January and November are comparable. The relatively small magnitude of the zonal momentum flux in November is due to the cancellation of positive and negative momentum fluxes in the monthly mean. The intrinsic phase velocity vectors by individual sounding in November (not shown) are mostly directed westward, but 10 among 48 soundings direct eastward with much larger magnitudes, and this is responsible for making small magnitude of the monthly-mean zonal momentum flux in November. The negative (positive) $\overline{u'w'}$ represents westward (eastward) propagating intrinsic phase velocities (see Fig. 8a) in order for wave energy to propagate upward. These estimates of $\overline{u'w'}$ are relatively smaller than those of $-0.2\,\mathrm{m^2\,s^{-2}}$ in wintertime and $-0.03\,\mathrm{m^2\,s^{-2}}$ in summertime by the MU radar (Murayama et al, 1994). This difference is likely due to the different properties of the waves observed between the two techniques. The radar focuses on higher frequencies and includes longer vertical wavelengths. The sign of $\overline{u'w'}$ in the present summertime is positive (even though its magnitude is very small). This is mainly due to the eastward propagating intrinsic phase velocity of gravity waves (Fig. 8a), which is different from Murayama et al. The magnitude of $\overline{v'w'}$ is generally smaller than that of $\overline{u'w'}$ except in November and December, and there is no strong seasonal variation of $\overline{v'w'}$. The small value of monthly-averaged $\overline{v'w'}$ in January and November is mainly due to cancellation by negative and positive $\overline{v'w'}$ for individual soundings in each month. Note that estimating momentum flux using rawinsonde data is highly dependent upon analysis method, so a great deal of uncertainty in the magnitude of momentum flux can exist.

3.5 Convective sources in summertime

In order to make sure whether there is a relationship between convection and wave activity, the time series of hourly precipitation amount observed at Pohang station and two nearby stations located at about 17 km west (Gigye) and 30 km southwest (Kyeongju) of Pohang station in July are shown in Fig. 11. The RMS amplitude of meridional wind perturbation at Pohang station averaged in the stratosphere is superimposed on each precipitation plot. Here, filled circles represent cases in which precipitation occurred at least at one of the three stations at or near the time of balloon launch. Some features can

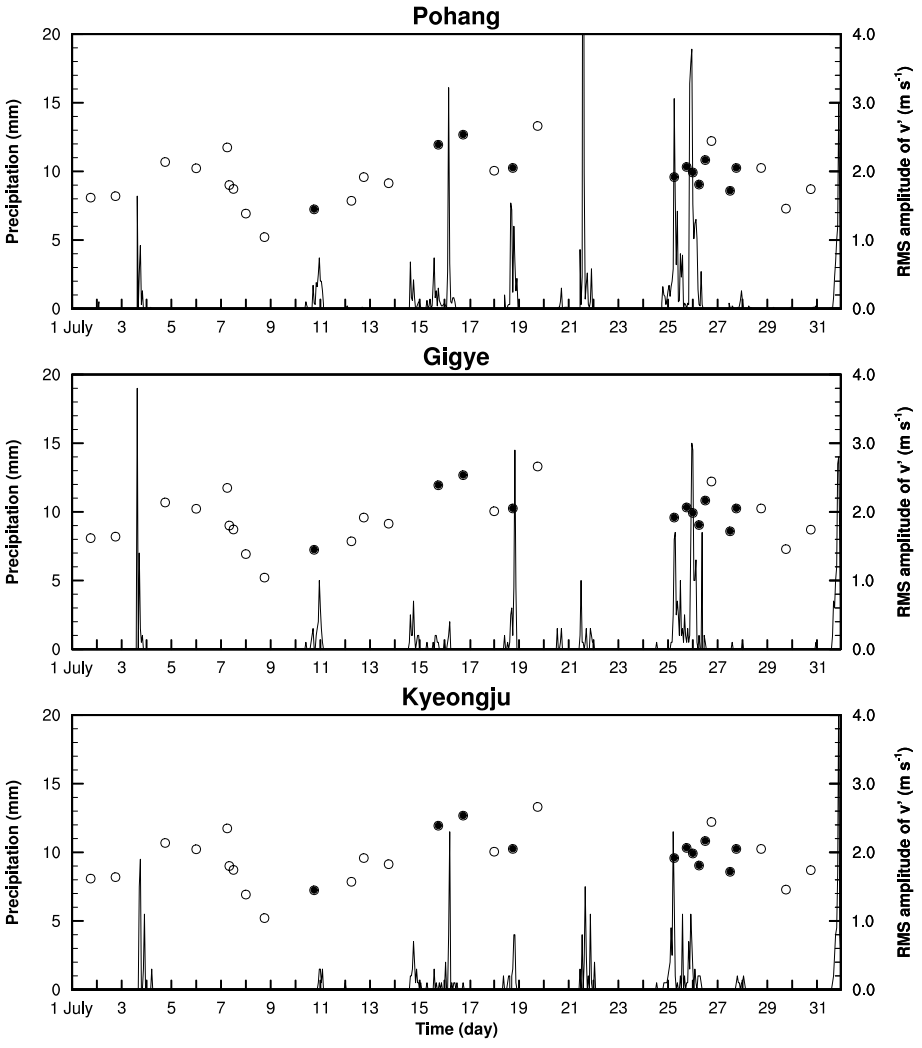

Fig. 11. Time series of hourly precipitation amount (mm) observed at Pohang, Gigye, and Kyeongju stations superimposed on meridional wind perturbation observed in rawinsondes at Pohang station (denoted by circles). Filled circles represent cases in which precipitation occurred at least at one of the three stations at or near the time when each rawinsonde balloon was launched

be found in Fig. 11. First, the temporal and spatial variations of precipitation amount are significant in hourly data. Even though the three stations are not far from each other, precipitation amount differs significantly, implying that the horizontal scale of convective cells producing precipitation might be very small ($\sim$10 km) and that convection is highly intermittent. Secondly, there is a possibility that the observed perturbation is not only due to convective sources at Pohang station but also those nearby. Since observed waves close to convective sources might have high frequencies and long vertical wavelengths, which are not well captured in rawinsonde data, observed waves with relatively low frequencies and short vertical wavelengths are likely due to convective sources nearby Pohang station. Under this situation, observed waves at Pohang station may result from a complex combination of multi-waves that are presumably generated by different convective sources at different locations. Thus, the characteristics of waves captured by balloons, which drift by basic-state wind, are strongly dependent on the location of balloons relative to convective sources.

Figure 12 shows estimated trajectories of balloons from the surface to $z = 30$ km and ground-based phase velocity in the stratosphere in the cases of the first (18 UTC, July 10, 1998) and fifth (06 UTC, July 25, 1998) filled circles shown in Fig. 11. Note that for these selected soundings precipitation occurred at all three stations when a balloon was launched. The balloon trajectories are estimated by integrating horizontal winds over 10-second intervals. The characters P, G, and K represent Pohang, Gigye, and Kyeongju stations, respectively. The numbers 17 km and

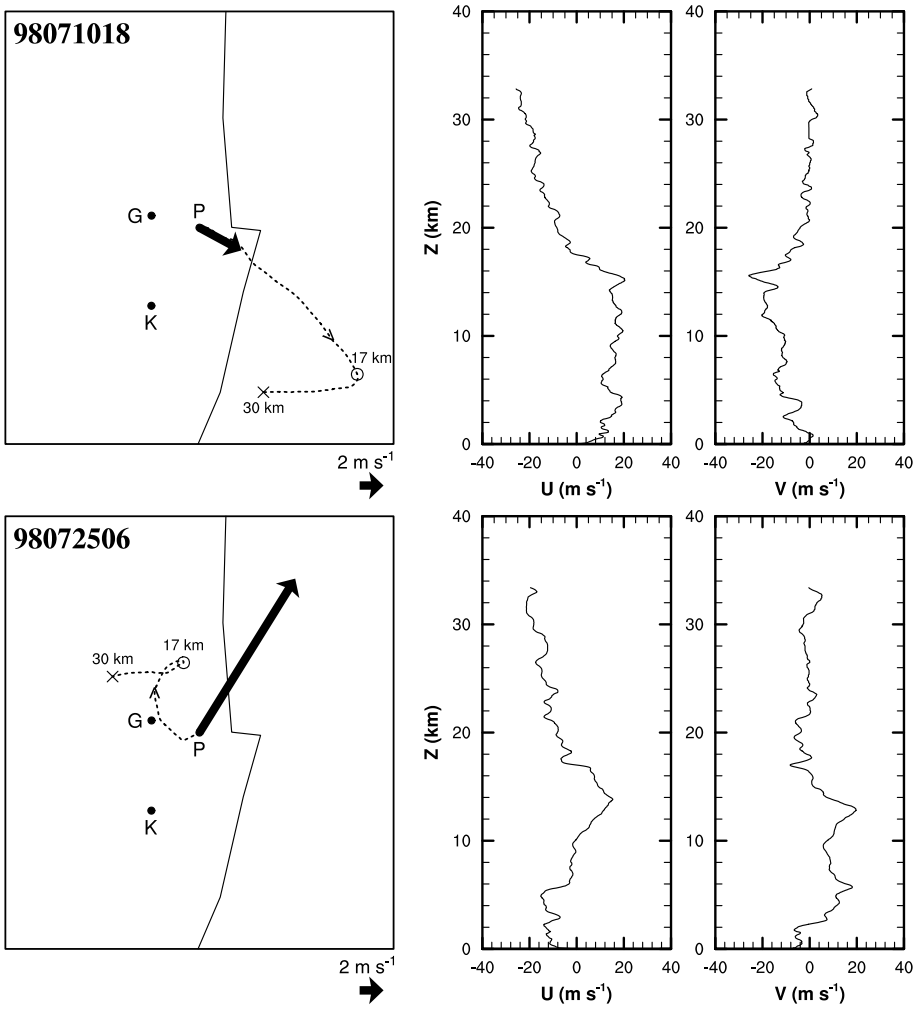

Fig. 12. Balloon trajectories (dashed curves) projected on a horizontal map around Pohang station and ground-relative phase velocity (thick arrows) in the stratosphere (17–30 km) (left) and zonal and meridional wind profiles (right two columns) in the cases of (**a**) the first filled circle (18 UTC 10 July 1998), and (**b**) the fifth filled circle (06 UTC 25 July 1998) shown in Fig. 11. P, G, and K denote Pohang, Gigye, and Kyeongju stations, respectively. The numbers on the map indicate heights

30 km indicate heights. In the first case, balloon drifted southeast of all three stations in the stratosphere mainly due to strong northwesterly wind in the troposphere. Therefore, waves observed in the stratosphere at Pohang station, which has a southeastward propagation direction, are presumably generated by convective sources at all-three stations. The characteristics of waves detected by a balloon depend on the location of convective sources relative to the balloon. If convective sources at each station are assumed to be fixed during balloon floating, waves generated at Gigye may have relatively low intrinsic frequencies and small vertical wavelengths compared with those generated at Kyeongju, in order to travel longer distance in a limited height range.

In the second case, balloon drifted northward and westward above $z = 17$ km. Thus, convective sources at Pohang may exist south and east of the balloon at all times during its floating in the stratosphere, while those at Gigye and Kyeongju exist south and west of the balloon in the lower stratosphere but east of the balloon in the upper stratosphere. Therefore, the balloon can capture gravity waves generated by convective sources at Pohang with westward and northward propagating components and at Gigye and Kyeongju with both westward and eastward propagating components in zonal direction and northward component. The observed waves at Pohang in the stratosphere (having a phase velocity in the northeast direction) can be due to convective sources at the nearby stations as well as Pohang station. Since the magnitude of phase speeds for westward propagating components must be very large to survive through critical-level filtering in an easterly zonal wind situation, those waves have relatively high intrinsic frequencies and large vertical wavelengths, which are not easy to be observed in rawinsondes. Therefore, the

dominant direction of phase speed in the stratospheric perturbation should be northeastward, as shown in the bottom panels of Fig. 12.

Considering that the characteristics of waves observed in rawinsondes are determined by a combination of waves generated by sources at nearby locations, further analysis including more stations nearby Pohang station will be necessary. In addition, it should be noted that gravity waves generated by multiple sources are superposed in the observation and that the wave superposition can possibly lead to errors in the interpretation of analysis results. Although the spectral analysis (e.g., the spectral Stokes parameter method) used in this study is based on the assumption that waves should be well separated from each other in the vertical wavenumber domain, such an assumption is not well justified in the real atmosphere where numerous waves generated by various sources exist. Therefore, uncertainties due to wave superposition will exist in the two cases shown in Fig. 12. In these two cases, however, the degree of polarization (Eckermann, 1996) for perturbations observed in the stratosphere is about 0.6. Given that the degree of polarization is a measure of the coherence of perturbations, which is unity for a monochromatic coherent wave, wave characteristics obtained in the two cases are believed to be more or less reliable.

4. Summary and conclusions

The characteristics of gravity waves and their temporal variations were investigated using rawinsonde data at Pohang observatory, Korea during the one-year period of 1998. The analysis of gravity waves was carried out for two atmospheric layers representing the troposphere (2–9 km) and stratosphere (17–30 km). The vertical profiles of temperature and horizontal wind perturbations and the hodograph of horizontal wind perturbations indicated that the observed perturbations in the stratosphere are upward propagating inertia-gravity waves generated below $z = 17$ km. The monthly-averaged root-mean-square amplitudes of temperature and wind perturbations in the stratosphere revealed strong seasonal variations, with their maxima in wintertime and minima in summertime. The time-height cross-section of perturbation energy showed that the large wave energy occurs near the subtropical jet region ($z = 14$–16 km), but correlation with the strength of the vertical gradient of static stability is not clear in any seasons.

It was shown that gravity waves propagate mainly westward in wintertime and northeastward in summertime relative to the mean wind, implying a significant degree of directional anisotropy. The intrinsic frequency was $2f$–$3f$ in the stratosphere and $3f$–$5f$ in the troposphere without any obvious seasonal variation. The vertical and horizontal wavelengths in the stratosphere ranged from 2.6 to 3.3 km and 310 to 530 km, respectively. The mean intrinsic phase velocity in the stratosphere was $8.4\,\mathrm{m\,s^{-1}}$ toward the west in January and $7.4\,\mathrm{m\,s^{-1}}$ toward the northeast in July. The evidence of the strong anisotropy of wave propagation was represented in the vertical flux of horizontal momentum. The zonal momentum flux was mostly negative except in summertime with a peak value of $-0.13\,\mathrm{m^2\,s^{-2}}$ in January and a minimum magnitude of $0.003\,\mathrm{m^2\,s^{-2}}$ in July. It is noteworthy that there is no unambiguous methodology to estimate momentum flux using rawinsonde data, so both the magnitude and seasonal variation of the monthly and vertically averaged momentum flux estimated in the present study inherently contain uncertainties.

In January, most of soundings have very small values of ground-based phase velocity when the horizontal wind in the lower troposphere is either northwesterly or southwesterly according to synoptic situations. This implies that topography can be a source of gravity waves in the winter stratosphere observed at Pohang observatory located on the east coast of Korea. In July, a possible relationship between convective activity and observed perturbation was investigated using hourly precipitation data at Pohang and other two nearby stations. It was found that convective activity is very much localized and intermittent. This implies that the characteristics of observed waves cannot be understood without considering a complex combination of waves generated by sources at different locations relative to balloons and the observational filtering of rawinsondes with limited depth and observing frequency.

There are several factors that can influence the present results. First, the results in summertime might be statistically less significant than other

times of the year because of less abundant data. Second, fixing the height and depth of the stratosphere and troposphere layers can raise some problem in the present study having strong seasonal variation of tropopause height. Especially, the lower limit of the summer stratosphere (17 km) may not be high enough to safely escape from erroneous effects on the power spectrum due to a sudden increase of static stability near the tropopause. Third, the calculated wave parameters are based on currently used analysis techniques under various assumptions, which might be not always realistic. One of them is the monochromatic assumption, which can lead to errors in the interpretation of analysis results when gravity waves generated by multiple sources are superposed in the observation. Fourth, balloon sounding gives an effective vertical profile for waves only when horizontal wavelengths of the waves are larger than the horizontal travel distance of balloon. Therefore, analysis results should be interpreted with caution, considering such a limitation of balloon observation. Finally, a question of whether seasonal variation of wave activity revealed in the present analysis is physically related to the temporal variation of wave sources or due to observational filtering by the basic state as also pointed out by Alexander (1998) and Vincent and Alexander (2000) may still remain. In spite of these problems, this study clearly demonstrates a usefulness of rawinsonde data in characterizing gravity waves and their seasonal variations.

Acknowledgments

The authors thank two anonymous reviewers for their comments that helped to improve the manuscript. This research was supported by Korea Research Foundation Grant (KRF-2001-DS0076) and by R02-2004-000-10027-0 from the Basic Research Program of the Korean Science and Engineering Foundation.

References

Alexander MJ (1998) Interpretations of observed climatological patterns in stratospheric gravity wave variance. J Geophys Res 103: 8627–8640

Alexander MJ, Holton JR (2004) On the spectrum of vertically propagating gravity waves generated by a transient heat source. Atmos Chem Phys Discuss 4: 1–27

Allen SJ, Vincent RA (1995) Gravity wave activity in the lower atmosphere: Seasonal and latitudinal variations. J Geophys Res 100: 1327–1350

Andrews DG, Holton JR, Leovy CB (1987) Middle atmosphere dynamics. New York: Academic Press, 489 pp

Chun H-Y, Song I-S (2001) Characteristics of inertia-gravity waves revealed in high-resolution radiosonde data at Pohang, Korea. J Korean Meteor Soc 37: 109–128

Dewan EM, Good RE (1986) Saturation and the "universal" spectrum for vertical profiles of horizontal scalar winds in the atmosphere. J Geophys Res 91: 2742–2748

Dewan EM, Gossard N, Quesada AF, Good RE (1984) Spectral analysis of 10 m resolution scalar velocity profiles in the stratosphere. Geophys Res Lett 11: 80–83

Eckermann SD (1995) On the observed morphology of gravity-wave and equatorial-wave variance in the stratosphere. J Atmos Terr Phys 57: 105–134

Eckermann SD (1996) Hodographic analysis of gravity waves: Relationships among Stokes parameters, rotary spectra and cross-spectral methods. J Geophys Res 101: 19169–19174

Eckermann SD, Vincent RA (1989) Falling sphere observations of anisotropic gravity wave motions in the upper stratosphere over southern Australia. Pure Appl Geophys 130: 509–532

Fritts DC, Alexander MJ (2003) Gravity wave dynamics and effects in the middle atmosphere. Rev Geophys 41: 1003 (DOI:10.1029/2001RG000106)

Fritts DC, Lu W (1993) Spectral estimates of gravity wave energy and momentum fluxes. Part II: Parameterization of wave forcing and variability. J Atmos Sci 50: 3695–3713

Fritts DC, VanZandt TE (1993) Spectral estimates of gravity wave energy and momentum fluxes. Part I: Energy dissipation, acceleration, and constraints. J Atmos Sci 50: 3686–3694

Hines CO (1989) Tropopausal mountain waves over Arecibo: A case study. J Atmos Sci 46: 476–488

Hines CO (1991) The saturation of gravity waves in the middle atmosphere. Part II: Development of Doppler-spread theory. J Atmos Sci 48: 1360–1379

Holton JR (1983) The influence of gravity wave breaking on the general circulation of the middle atmosphere. J Atmos Sci 40: 2497–2507

Holton JR, Wehrbein WM (1980) A numerical model of the zonal mean circulation of the middle atmosphere. Pure Appl Geophys 108: 284–306

Karoly DJ, Roff GL, Reeder MJ (1996) Gravity wave activity associated with tropical convection detected in TOGA COARE sounding data. Geophys Res Lett 23: 261–264

Kitamura Y, Hirota I (1989) Small-scale disturbances in the lower stratosphere revealed by daily rawinsonde observations. J Meteor Soc Japan 67: 817–831

Korea Meteorological Administration (2000) Enhanced rawinsonde observation in Korea. KMA, 162 pp

Leovy CB (1964) Simple models of thermally driven mesospheric circulation. J Atmos Sci 21: 327–341

Lindzen RS (1981) Turbulence and stress owing to gravity wave and tidal breakdown. J Geophys Res 86: 9709–9714

Matsuno T (1982) A quasi one-dimensional model of the middle atmosphere circulation interacting with internal gravity waves. J Meteor Soc Japan 60: 215–227

Medvedev AS, Klaassen GP (1995) Vertical evolution of gravity wave spectra and the parameterization of associated wave drag. J Geophys Res 100: 25841–25853

Murayama Y, Tsuda T, Fukao S (1994) Seasonal variation of gravity wave activity in the lower atmosphere observed with the MU radar. J Geophys Res 99: 23057–23069

Nappo CJ (2002) An introduction to atmospheric gravity waves. New York: Academic Press, 276 pp

Norton WA, Thuburn J (1999) Sensitivity of mesospheric mean flow, planetary waves, and tides to strength of gravity wave drag. J Geophys Res 104: 30897–30912

Ogino S, Yamanaka MD, Fukao S (1999) Interannual and day-to-day variations of gravity wave activity in the lower stratosphere over the eastern part of Japan observed in winter 1989–95. J Meteor Soc Japan 77: 413–429

Press WH, Teukolsky SA, Vetterling WT, Flannery BP (1992) Numerical recipes: The art of scientific computing, 2nd ed. Cambridge University Press, 963 pp

Sato K (1994) A statistical study of the structure, saturation and sources of inertio-gravity waves in the lower stratosphere observed with the MU radar. J Atmos Terr Phys 56: 755–774

Sato K, Kumakura T, Takahashi M (1999) Gravity waves appearing in a high-resolution GCM simulation. J Atmos Sci 56: 1005–1018

Tsuda T, VanZandt TE, Mizumoto M, Kato S, Fukao S (1991) Spectral analysis of temperature and Brunt-Vaisala frequency fluctuation observed by radiosondes. J Geophys Res 96: 17265–17278

VanZandt TE (1982) A universal spectrum of buoyancy waves in the atmosphere. Geophys Res Lett 9: 575–578

Vincent RA (2003) Status of the SPARC radiosonde initiative, SPARC Newsletter, No 20, January 2003

Vincent RA, Alexander MJ (2000) Gravity-waves in the tropical lower stratosphere: An observational study of seasonal and interannual variability. J Geophys Res 105: 17971–17982

Vincent RA, Allen SJ, Eckermann SD (1997) Gravity-wave parameters in the lower stratosphere. Gravity wave processes and their parameterization in global climate models. Springer, 404 pp

Wang L, Geller MA (2003) Morphology of gravity-wave energy as observed from 4 years (1998–2001) of high vertical resolution U.S. radiosonde data. J Geophys Res 108: 4489 (DOI:10.1029/2002JD002786)

Warner CD, McIntyre ME (1996) On the propagation and dissipation of gravity wave spectra through a realistic middle atmosphere. J Atmos Sci 53: 3213–3235

Weinstock J (1990) Saturated and unsaturated spectra of gravity waves and scale-dependent diffusion. J Atmos Sci 47: 2211–2225

Corresponding author's address: Hye-Yeong Chun, Department of Atmospheric Sciences, Yonsei University, Seoul 120-749, Korea (E-mail: chy@atmos.yonsei.ac.kr)

Verleger: Springer-Verlag GmbH, Sachsenplatz 4–6, 1201 Wien, Austria. – Herausgeber: Prof. Dr. Reinhold Steinacker, Institut für Meteorologie und Geophysik, Universität Wien, Althanstraße 14, 1090 Wien, Austria. – Redaktion: Althanstraße 14, 1090 Wien, Austria. – Satz und Umbruch: Thomson Press (India) Ltd., Chennai. – Druck und Bindung: Grasl Druck&Neue Medien, 2540 Bad Vöslau, Austria. – Verlagsort: Wien. – Herstellungsort: Bad Vöslau. – Printed in Austria.